ECOHYDROLOGY
Ecohydrol. **4**, 394–410 (2011)
Published online 25 June 2010 in Wiley Online Library
(wileyonlinelibrary.com) DOI: 10.1002/eco.141

Effects of lateral hydrological processes on photosynthesis and evapotranspiration in a boreal ecosystem

Ajit Govind,[1,2]* Jing Ming Chen,[2] Jeffery McDonnell,[3] Jyothi Kumari[1] and Oliver Sonnentag[4]

[1] *Unité de Recherche en Ecologie Fonctionnelle et Physique de l'Environnement (EPHYSE), INRA, Villenave d'Ornon, France*
[2] *Department of Geography and Program in Planning, University of Toronto, ON, Canada*
[3] *Department of Forest Engineering, Oregon State University, 97331, OR, USA*
[4] *Department of Organismic & Evolutionary Biology, Harvard University, 02138, MA, USA*

ABSTRACT

Landscape-scale hydrological processes can greatly alter the local-scale water balance and many ecological processes linked to it. We hypothesized that in humid forest ecosystems, topographically driven lateral subsurface flow (SSF) has significant influence on ecophysiological processes such as gross primary productivity (GPP) and evapotranspiration (ET). To investigate how simplified hydrological conceptualizations influence the simulated ET and GPP in space and time, we conducted a numerical experiment using a spatially explicit hydroecological model, BEPS-TerrainLab V2.0. We constructed three modelling scenarios: (1) *Explicit*, where a realistic calculation of SSF was employed considering topographic controls, (2) *Implict*, where the SSF calculations were based on a bucket-modelling approach and (3) *NoFlow*, where the SSF was turned-off in the model. Statistical analyses of model outputs showed considerable differences among the three scenarios for the simulated GPP and ET. The *NoFlow* scenario generally underestimated GPP and ET, while the *Implicit* scenario overestimated them relative to the *Explicit* scenario, both in time and space. GPP was more sensitive to SSF than ET because of the presence of unique compensatory mechanisms associated with the subcomponents of the total ET. The key mechanisms controlling GPP and ET were manifested through nonlinear changes in stomatal conductance, unique contributions from GPP and ET subcomponents, alterations in rhizosphere wetting patterns and their impacts on upscaling mechanisms and variability in nitrogen dynamics (for GPP). Feedback and interactive relationships between hydrological and ecophysiological processes also exacerbated the biases. Thus, we conclude that ecological models that have simplified hydrological representations could have significant errors in the estimation of GPP and ET. Copyright © 2010 John Wiley & Sons, Ltd.

Supporting information may be found in the online version of this article.

KEY WORDS spatially explicit hydroecological modelling; hydrological conceptualizations; ecophysiological and hydrological coupling; boreal ecosystems; gross primary productivity; evapotranspiration

Received 10 December 2009; Accepted 6 May 2010

INTRODUCTION

Much of the uncertainty in quantifying how changes in climate will alter ecophysiological and biogeochemical processes in different ecosystems is linked to our rudimentary understanding of landscape-scale hydrological processes and how it influences biogeochemical processes (Gedney *et al*., 2006; Zimov *et al*., 2006). Ecophysiological and biogeochemical processes vary in space and time due to the heterogeneities in the local-scale hydrothermal conditions. Consequently, dynamics of the soil-plant-atmopheric-continuum (SPAC) of mass and energy are highly nonlinear and dominated by thresholds and feedbacks (Joos *et al*., 2001; Porporato *et al*., 2003; Daly *et al*., 2004; Sitch *et al*., 2005; Manzoni and Porporato, 2007). In humid landscapes, much of the variation in soil water is driven by lateral water fluxes (McDonnell *et al*., 2007; Rodriguez-Iturbe *et al*., 2007). While ambient soil moisture is the net result of the magnitudes of various components of the water balance, hill-slope hydrological processes that drive lateral flow are often neglected in most of the ecological models (e.g. Running *et al*., 1994; Potter *et al*., 2001; Arain *et al*., 2006; Coops *et al*., 2007) and in land surface schemes (LSS) that are used within global general circulation models (e.g. Mihailovic *et al*., 1993; Polcher *et al*., 1995 Cox *et al*., 1999). Recently, Morales *et al*. (2005) has shown that most of the ecosystem models inadequately simulated ecophysiological and biogeochemical processes because of the incompleteness in their representations of hydrological processes.

Hydrological and ecological models differ greatly in their representation of soil-water dynamics (Rodriguez-Iturbe, 2000). While ecological models often ignore or simplify the amount of water that drains laterally across the landscape (Turner *et al*., 2006; Coops *et al*., 2007), conventional hydrological models often focus only on lateral water redistribution during and between events and greatly simplify vegetation controls on soil moisture dynamics (Beven *et al*., 1984; Armstrong and Martz, 2003; Koster *et al*., 2006; Vazquez and Feyen, 2007).

* Correspondence to: Ajit Govind, Ecologie Fonctionnelle et Physique de l'Environnement (EPHYSE), L'Institut national de la recherche agronomique, 71 Avenue Edouard Bourlaux, 33140 Villenave d'Ornon, France. E-mail: ajit.govind@bordeaux.inra.fr

Most of the one-dimensional ecosystem models (Arora and Boer, 2006; Grant *et al*., 2006) explicitly simulate key plant and biogeochemical processes but often simulate only vertical hydrological processes without consideration of lateral hydrological processes and redistribution. Even in spatially distributed ecological models that use remotely sensed data, the modelling units (pixels) are one-dimensional representation of the SPAC and hence the lateral hydrological processes are simplified. In these approaches, soil moisture controls are represented as 'available soil moisture' (e.g. Liu *et al*., 1997) or in the form of scalars that represent hydrological controls on vegetation (e.g. Heinsch *et al*., 2006; Coops *et al*., 2007). Indeed, Ju *et al*. (2006) have noted that almost none of the regional-scale ecological models include the mechanistic redistribution of soil water. We believe that such simplified hydrological representations could contribute to significant errors in the simulated ecophysiological processes such as photosynthesis and evapotranspiration (ET).

Here we examine the effects of lateral hydrological processes on photosynthesis and ET in a boreal ecosystem. High latitude boreal forests play a major role in global climate dynamics (Thompson *et al*., 1996; Chen *et al*., 2003). Because the majority of fresh water resources (including ice and snow) are located in high latitudes, these ecosystems play a major role in the global climate dynamics (Thompson *et al*., 1996; Chen *et al*., 2003). Our overall goal was to explore how much hydrological detail is required in an ecological model in order to realistically simulate ecophysiological and biogeochemical processes.

We used the spatially explicit model, BEPS-TerrainLab V2.0 model (Govind *et al*., 2009a), as a framework for a numerical experiment (Weiler and McDonnell, 2004) to explore the hydrological impacts on ecophysiological processes in a boreal ecosystem. We constructed modelling scenarios that differed in the level of complexity with which lateral hydrological processes are conceptualized in conventional ecological models and their performances were evaluated. We focused on the spatio-temporal distribution of the two main ecohydrological indicators: gross primary productivity (GPP) and ET. The objectives of this study were to investigate how hydrological simplifications contribute to biases in the simulated ET and GPP in space and time and to understand the mechanisms that create these biases.

SITE DESCRIPTION

Our numerical experiment focused on a 50 km^2 boreal watershed that includes the Eastern Old Black Spruce (EOBS) site of the Canadian Carbon Program (CCP), located at 49·69 °N and 74·34 °W, ~200 km northwest of the Lac St. Jean, Quebec, Canada (Figure 1). This region lies within the humid continental subarctic boreal

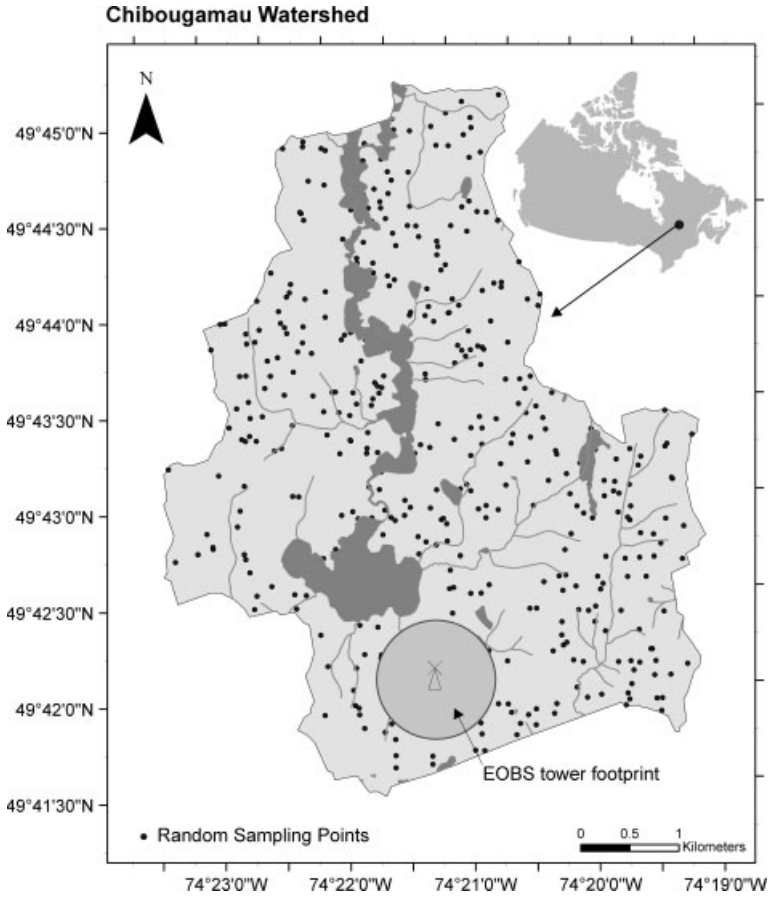

Figure 1. Location of the Chibougamau watershed, a humid boreal ecosystem, for which the numerical experiment was conducted.

DOI: 10.1002/eco

biome. Since mid-2003, an eddy covariance (EC) tower at EOBS has been making continuous high precision measurements of the fluxes of mass and energy between the landscape and the atmosphere. Details on the flux and meteorological measurements can be found in Bergeron *et al.* (2007, 2008). Black spruce (*Picea mariana*) is the dominant species in this boreal ecosystem. Paper birch (*Betula papyrifera Marsh.*) and aspen (*Populus balsamifera L.*) can also be found on elevated locations along esker ridges. The soil is predominantly a podzol, covered by an organic layer with an average depth of 26–30 cm. In humid locations where the soil is predominantly 'organic', peat can occur as deep as 125 cm (Giasson *et al.*, 2006).

The total annual precipitation (P) of the study site (30-year trend) is ~950 mm (Environment Canada, 2006), two-thirds of which is approximately comprised of rainfall and one-third snowfall (Bergeron *et al.*, 2007). Approximately 27% of P is partitioned as ET and ~72% of P is partitioned as runoff. The remaining 1% of P alter the storage in the soil, affecting the volumetric soil moisture content (VSMC) and water table depth (WTD).

MATERIALS AND METHODS

BEPS-TerrainLab V2.0 is a spatially explicit model that simulates the hydrological, ecophysiological and biogeochemical processes and the related feedback relationships in a tightly coupled manner. A detailed description of this model can be found in Govind *et al.* (2009a,b).

Modelling of stomatal conductance

In a spatially explicit modelling approach, a practical method to calculate stomatal conductance (g_s) is to use a Jarvis (1976)-like algorithm wherein a species-specific maximum stomatal conductance ($g_{s,max}$) is constrained by a set of factors to return g_s. In BEPS-TerrainLab V2.0, g_s is calculated by a Jarvis (1976)-like scheme. In order to adequately represent plant–water relations in BEPS-TerrainLab V2.0, it is assumed that a canopy is comprised of physiologically distinct leaf types, based on the variability of resource factors, light and water. A canopy-scale ecophysiological process such as photosynthesis is contributed by physiologically distinct leaf types that have unique g_s values. Here, variability in light and soil moisture are considered as factors that govern intra-canopy physiological variability. Other factors such as relative humidity, soil temperature and air temperature also contribute to the dynamics of g_s. Scalars (ranging between 0 and 1) representing various environmental factors constrain a land cover-specific maximum stomatal conductance, $g_{s,max}$, to return the g_s as shown below:

$$g_s = g_{s\ max}.\left[f_a(F_p) \times f_b(T_a) \times f_c(D_v) \times f_d(\theta_{sw}) \times f_e(T_s)\right] \quad (1)$$

Here F_p is the photosynthetic photon flux density, T_a the mean air temperature, D_v the vapour pressure deficit, θ_{sw} the VSMC and the functions f_{a-e} are factor-specific functions. Unlike water-limited ecosystems, where plant stress is a direct function of water scarcity, in humid boreal ecosystems, water stress is mostly attributed to soil saturation (flooding). There are many studies that provide evidence that either g_s decreases with increasing θ_{sw} beyond the field capacity (Kozlowski, 1984; Else *et al.*, 1996). This may be because of soil saturation-induced plant stress that occurs because of a variety of reasons such as anoxic conditions and production of toxic compounds in the rhizosphere. In order to conceptualize this, in BEPS-TerrainLab V2.0 we use a $f(\theta_{sw})$ which is unique to boreal ecosystems. The method for calculating these scalars can be found in Chen *et al.* (2005) and Sonnentag *et al.* (2008). In BEPS-TerrainLab V2.0, a new scalar $f(T_s)$ accounts for the effects of soil temperature on g_s. This scalar is robust to capture the plant physiological enhancement during the spring, even though the air temperature remains physiologically suboptimal (Govind *et al.*, 2009a). Finally, the total conductance is calculated by assuming the cuticular conductance ($g_{cuticle}$) in parallel and boundary layer conductance ($g_{boundary}$) in series to g_s, such that the total conductance for water vapour exchange becomes

$$g_{total} = \frac{g_{boundary} \times (g_{cuticle} + g_s)}{g_{boundary} + g_{cuticle} + g_s} \quad (2)$$

For the moss layer, the surface conductance is calculated using a least squares regression after Williams and Flanagan (1998) and for soil it is calculated as a direct function of VSMC.

Conductance for CO_2 transport between the vegetation and the atmosphere is assumed to be 0·0625 times the conductance for H_2O.

Modelling ecohydrological processes

ET is calculated as the sum of evaporation and transpiration using the Penman–Monteith (PM) equation and GPP is calculated using the temporally integrated Farquhar model (TIFM) of Chen *et al.* (1999), for different canopy layers (overstory and understory), moss and soil surface, using surface-specific microclimatic variables and parameters.

Leaf-level processes (GPP and ET) are upscaled to the canopy using fractions of leaf area index (LAI) as weighting terms that correspond to variability in canopy physiological status due to the two main resources, light and water. BEPS-TerrainLab V2.0 employs a modified sunlit-shaded leaf strategy, i.e. the *four-leaf approach* to spatially upscale leaf-level ecophysiological processes to the canopy scale by assuming that within each light regime there are two states of moisture regimes, i.e. canopy is comprised of four physiologically distinct leaf types based on the differences in light and water status. For example, for overstory canopy transpiration (T_o), firstly, leaf-level ecophysiological processes are calculated using unique g_s (for water vapour) and then

DOI: 10.1002/eco

upscaled to the canopy as shown below:

$$T_o = [T_{sun,unsat}\mathrm{LAI}_{over,sun}.\mu + T_{sun,sat}\mathrm{LAI}_{over,sun}(1-\mu)] + [T_{shade,unsat}\mathrm{LAI}_{over,shade}.\mu + T_{shade,sat}.\mathrm{LAI}_{over,shade}(1-\mu)] \quad (3)$$

where

$$T_{sun,sat} = f_1[R_{nsun},\ g_{s,sun,sat_{(\phi)}}]$$
$$T_{sun,unsat} = f_1[R_{nsun},\ g_{s,sun,unsat_{(\theta)}}]$$
$$T_{shade,sat} = f_1[R_{nshade},\ g_{s,shade,sat_{(\phi)}}]$$
$$T_{shade,unsat} = f_1[R_{nshade},\ g_{s,shade,unsat_{(\theta)}}] \quad (4)$$

The function f_1 is the PM equation, which uses leaf-specific net radiations (R_n) and g_s (for H_2O). In this scheme, it is assumed that the rhizosphere wetting patterns proportionately influence the physiological variability of the canopy. This is manifested through the variable μ (after Gale and Grigal, 1987), the fraction of roots in the unsaturated zone, and $(1-\mu)$, the fraction of roots in the saturated zone. The evaporation from the forest floor (E_{floor}) is calculated as the weighted sum of moss evaporation (E_{moss}) and soil evaporation (E_{soil}) which is calculated using the PM equation using surface-specific conductance values.

Similar to transpiration, photosynthesis is spatially upscaled using LAI fractions that correspond to different leaf physiological statuses as shown below:

$$A_o = [A_{sun,unsat}\mathrm{LAI}_{sun}.\mu + A_{sun,sat}\mathrm{LAI}_{sun}(1-\mu)] + [A_{shade,unsat}\mathrm{LAI}_{shade}.\mu + A_{shade,sat}.\mathrm{LAI}_{shade}(1-\mu)] \quad (5)$$

where

$$A_{sun,sat} = f_2[R_{s,sun},\ g_{s,sun,sat_{(\phi)}}]$$
$$A_{sun,unsat} = f_2[R_{s,sun},\ g_{s,sun,sat_{(\theta)}}]$$
$$A_{shade,sat} = f_2[R_{s,shade},\ g_{s,shade,sat_{(\phi)}}]$$
$$A_{shade,unsat} = f_2[R_{s,shade},\ g_{s,shade,unsat_{(\theta)}}] \quad (6)$$

In the Equation (5), A_o is the overstory canopy's photosynthesis which has subcomponents that are calculated using different combinations of radiation (R_s) and moisture regimes, based on the function, f_2, which is the TIFM.

For the understory canopy, however, for both transpiration and photosynthesis, a *quasi-big-leaf approach* is employed as the upscaling strategy, using a canopy conductance $g_{c,under}$, which is simply calculated as $g_{sunder} \times \mathrm{LAI}_{under}$. However, the relative understory contributions from the saturated and unsaturated zones are explicitly considered and are proportionately weighted. The understory transpiration and photosynthesis are expressed as:

$$T_{under} = [T_{under}.\mu_{under}] + [T_{under}.(1-\mu_{under})] \quad (7)$$

$$A_{under} = [A_{under}.\mu_{under}] + [A_{under}.(1-\mu_{under})] \quad (8)$$

Moss photosynthesis (A_{moss}) is calculated using the function f_2 but without any spatial upscaling mechanism because it is assumed to be single layered.

Other related processes such as soil heat transfer and hydrothermally controlled soil biogeochemical processes are also considered in BEPS-TerrainLab V2.0. Soil temperature at various depths is calculated by numerically solving the Fourier heat transfer process using the Crank–Nicholson scheme for a six-layered soil profile (one dynamic snow layer and five soil layers). Explicit modelling of soil carbon (C) and nitrogen (N) dynamics as a function of soil water and soil temperature facilitate the detailed modelling of biogeochemical processes.

Water balance of a BEPS-TerrainLab V2.0 modelling unit

Most of the hydrological processes are conceptualized in BEPS-TerrainLab V2.0 by solving a detailed water balance equation that considers lateral water fluxes, saturated zone and unsaturated zone hydrological processes, snow dynamics and canopy hydrological processes, at a daily time step.

The local-scale water balance is conceptualized on a per-pixel basis. The soil is divided into the saturated and unsaturated zones. For a given pixel, the water balance in the unsaturated zone at a daily time step can be expressed as:

$$\Delta W_{unsat} = I - R_{SOLF} + W_{cr} - W_{pe} - T_{o,unsat} - T_{u,unsat} - E_{floor} \quad (9)$$

where ΔW_{unsat} is the storage change in the unsaturated zone; I the net precipitation that reaches the soil surface and is composed of throughfall, stemflow and snowmelt; R_{SOLF} the surface overland flow (SOLF); W_{cr} the capillary rise from the saturated zone to the unsaturated zone; W_{pe} the percolation from the unsaturated zone to the saturated zone; $T_{o,unsat}$ the overstory transpiration (water consumed by roots lying in the unsaturated zone); $T_{u,unsat}$ the understory transpiration (water consumed by roots lying in the unsaturated zone) and E_{floor} the forest floor evaporation (weighted sum of soil and moss evaporation) and/or the sublimation from the forest floor snow pack.

For a given pixel, in the saturated zone, the water balance at a daily time step is

$$\Delta W_{sat} = W_{pe} - R_{ssf} - T_{o,sat} - T_{u,sat} - W_{cr} \quad (10)$$

where ΔW_{sat} is the storage change in the saturated zone; R_{ssf} the subsurface flow; $T_{o,sat}$ the overstory transpiration (water consumed by roots lying in the saturated zone); and $T_{u,unsat}$ the understory transpiration (water consumed by roots lying in the saturated zone).

The net water balance of the pixel as a whole is the sum of the storage change in the unsaturated and the saturated zones, ΔW, i.e. combining Equations (9) and (10) as shown below:

$$\Delta W = I - R_{SOLF} - R_{ssf} - T_{o,unsat} - T_{o,sat} - T_{u,unsat} - T_{u,sat} - E_{floor} \quad (11)$$

DOI: 10.1002/eco

Datasets used

We used various spatial and meteorological datasets to run the model in order to perform this numerical experiment. These spatial datasets include land cover, LAI, a hydrologically corrected digital elevation model, slope, aspect, soil texture, initial WTD, spatial distributions of the sizes and C : N ratios of the 13 conceptual C-pools in the ecosystem (i.e. 26 maps) and a watershed boundary. All of these spatial datasets had a common spatial resolution of 25 m in the UTM Z-18N projection.

Daily meteorological variables such as the maximum temperature, minimum temperature, dew point temperature, incoming shortwave radiation, wind speed and precipitation (rain or snow) were collected at one point (EOBS tower site) and were assigned to all the pixels in the modelling domain after correcting for the effects of elevation and slope on temperature and solar radiation, respectively. Biophysical and soil hydraulic parameters were assigned in a spatially explicit manner based on the land cover and soil maps, respectively Govind *et al.* (2009a,b).

In this study for model evaluation, EC measurements of the fluxes of water and C at the EOBS were used. EC datasets were quality controlled, gap filled and partitioned for flux subcomponents by Bergeron *et al.* (2007) using a standard Fluxnet-Canada algorithm developed by Barr *et al.* (2004). The CO_2 flux data after flux partitioning provided GPP estimates. These datasets were obtained from the Data Information System of the CCP (http://fluxnet.ccrp.ec.gc.ca/). We converted the latent heat flux measurements (W m^{-2}) to ET (mm day^{-1}) for model evaluation.

Numerical experiments

BEPS-TerrainLab V2.0 has been previously tested for 2 years using measurements of GPP, ET, WTD, VSMC (Govind *et al.*, 2009a), snow depth, soil temperature, total ecosystem respiration and net ecosystem exchange (Govind *et al.*, 2009b). In this study, we used the original model that has explicit hydroecological representation and then compared its simulations to the ones with progressively simpler hydrological conceptualizations to investigate how hydrological representation of lateral flow affects the simulated magnitudes of GPP and ET. Such lateral flows at the watershed scale could be either due to surface or subsurface flows. Infiltration-excess overland flow (Horton, 1933) is a rare phenomenon at the study site due to the very high infiltration capacities. While surface overland flow (SOLF) (Dunne and Black, 1970) sometimes occurs under unusually wet conditions when the WTD is at the soil surface, its appearance is also quite limited. Many field-based studies have shown that in boreal ecosystems, the dominant process for lateral water distribution is the topographically driven subsurface flow (SSF) (Renzetti *et al.*, 1992; Weiler *et al.*, 2005; McEachern *et al.*, 2006), which plays a significant role in regulating the local-scale water balance.

To investigate the differences in the simulated ecophysiological processes due to variations in the conceptualizations of local hydrological regimes, we designed three modelling scenarios (Figure 2, Table I) that differed only in the complexity with which SSF was modelled. All spatial and meteorological datasets, parameter values and initialization procedures were kept the same in all the scenarios as in Govind *et al.* (2009a), in order to study the ecohydrological interactions due to differences in the hydrological conceptualizations.

1. The *Explicit* scenario: This scenario includes both forms of lateral water fluxes, i.e. SSF and SOLF as a function of topography, as outlined in Govind *et al.* (2009a). Here SSF is calculated based on a depth-integrated Darcy's approach (Wigmosta *et al.*, 1994; Chen *et al.*, 2005) using soil-specific transmissivity schemes. However, unlike most of the hydroecological models where topographic slope is used, the slope of the WTD (hydraulic head), updated on a daily basis, is used to calculate SSF. Considering the critical role of preferential water fluxes in forested ecosystems (Weiler and McDonnell, 2007), a peat-specific transmissivity scheme is used to describe the preferential water fluxes through the peat necromass. The SSF calculated in this manner is exchanged with the neighbouring

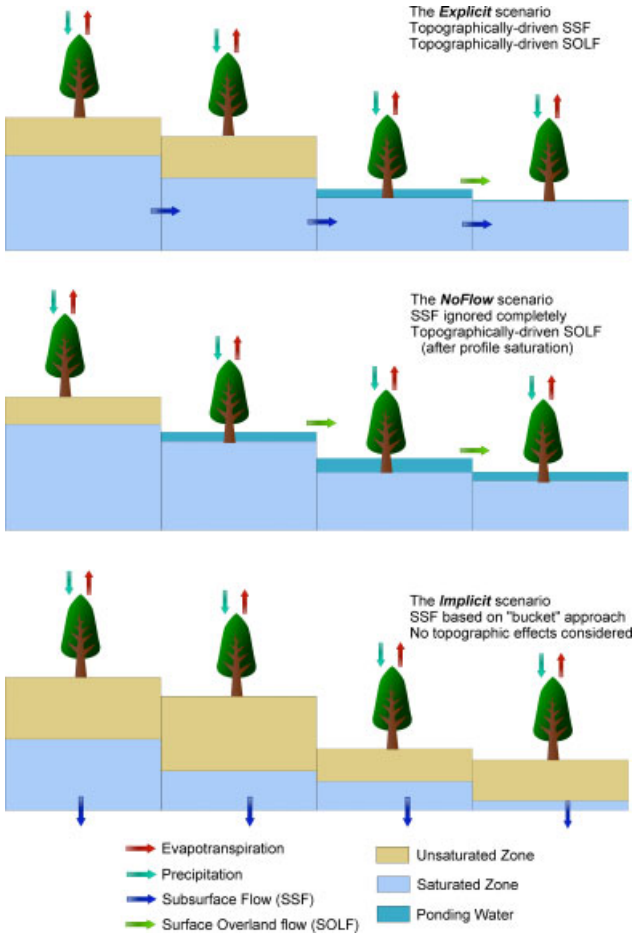

Figure 2. Conceptual representation of various hydrological scenarios considered in this study.

DOI: 10.1002/eco

Table I. Characteristic features of the three hydrological scenarios considered in this numerical experiment.

Features	Scenarios		
	Explicit	*Implicit*	*NoFlow*
SSF	Realistic	Accounted	NA[a]
SOLF	Possible	Rare	Dominant
Soil profile saturation	Optimal	Hyperoptimal	Hypooptimal
Routing of SSF	Present	Absent	Absent
Routing of SOLF	Present	Absent	Present
Effect of topography	Considered	Ignored	Considered[b]
Rhizophere saturation[c]	$0 < \mu < 1$	$\sim \mu = 1$	$\sim \mu = 0$
Nutrient availability	Accurate	Intensified	Suppressed
Presence in Ecological models	Not common	Common[d]	Common[e]

[a] Not at all considered in this scenario.
[b] SOLF drains-off based on topography after soil storage is filled up.
[c] Fraction of rhizosphere lying in the unsaturated zone (μ) or saturated ($1 - \mu$) is quantified using a root geometry parameter (ρ) and WTD, after Gale and Grigal (1987).
[d] Liu *et al*. (1997a); Potter *et al*. (2001); Heinsch *et al*. (2006); Coops *et al*. (2007).
[e] Many LSS within GCMs that consider topographically driven SOLF but not SSF (Verseghy, 1991; Dickinson *et al*., 1992; Mihailovic *et al*., 1993; Polcher *et al*., 1995; Cox *et al*., 1999).

pixels which in turn affects the water balance of the neighbouring pixels and itself. When the WTD reaches the ground surface, water gets 'ponded' and is routed laterally as SOLF, which enters the water balance calculation of the neighbouring pixels as input components. This *Explicit* scenario represents the most detailed form of ecohydrological conceptualization in this experiment. Similar representations can be found in models such as RHESSys (Tague and Band, 2004) and VIC (Liang *et al*., 1994).

2. The *Implicit* scenario: In this scenario, the SSF is 'accounted' assuming a bucket-modelling scheme without any topographic influence and hence pixel-to-pixel exchange of SSF is absent. Theoretically, when the soil-water potential lies above the field capacity, its energy status is adequate for gravitational flow. Considering this, in the *Implicit* scenario, it is assumed that on a daily basis, some amount of water is drained as SSF from a given saturated zone depth. This SSF is equivalent to water that should be lost in order to reach a field capacity condition for that saturated zone depth. The remaining amount of water determines the new saturated zone depth and hence the WTD in the next time step. This assumption is currently used directly or indirectly in many of the ecological models that simplify soil hydrological processes. In the *Implicit* scenario, SSF is calculated as:

$$R_{\mathrm{ssf,implicit}} = [\theta_{\mathrm{s}} - \theta_{\mathrm{fc}}] \cdot d \qquad (12)$$

where $R_{\mathrm{ssf,implicit}}$ (mm day^{-1}) is the SSF calculated using the *Implicit* scenario; θ_{s} the VSMC at saturation ($\theta_{\mathrm{s}} = \phi$, porosity of the soil); θ_{fc} the VSMC at the field capacity and d the depth of the saturated zone, the difference between the depth of the soil profile and WTD, measured from the ground surface. The SSF calculated in this way is directly removed from a given pixel on a daily basis, thus affecting its water balance without affecting the water balance of the neighbouring pixels. Since there are neither topographic controls nor the effects of neighbouring pixels in this scenario, SSF is greatly simplified and consequently the soil always tends to maintain a water status below the field capacity. It seldom saturates the entire soil profile unless a very heavy precipitation event occurs especially at those locations where the soil storage is very small (e.g. a shallow soil profile). Thus, the probability of getting SOLF is almost negligible in this scenario. This 'implicit approach' is commonly used in most of the large-scale ecological models where simplified hydrological representations are adopted (e.g. BEPS, Liu *et al*., 1997; CASA, Potter *et al*., 2001; C-Flux, Turner *et al*., 2006).

3. The *NoFlow* scenario: This scenario assumes that there is no SSF between the pixels. The infiltrated soil water either evaporates or transpires. However, if the WTD reaches the soil surface, after filling the soil storage, a surface 'ponding' of water causes an 'overflow' of water, when SOLF is initiated. SOLF enters the water balance calculation of the neighbouring pixels. This type of approach is adopted in some of the LSS that are used within the global circulation models (e.g. Polcher *et al*., 1995; Shao and Henderson-Sellers, 1996; Cox *et al*., 1999; Comer *et al*., 2000). A key point is that in the *NoFlow* scenario, SOLF occurs only after the entire soil profile is saturated before the 'overflow' process occurs.

In summary, the *Explicit* scenario has topographically driven SSF that is exchanged with neighbouring pixels, the *Implicit* scenario has SSF implicitly calculated without topography and is not exchanged with the neighbouring pixels in the *NoFlow* scenario, SSF is fully ignored. In all the three scenarios, there is provision for SOLF pathway, although its occurrence is highly dependent on subsoil hydrological processes. In this article the *Implicit* and the *NoFlow* scenarios are collectively referred to as 'non-explicit' scenarios.

DOI: 10.1002/eco

Statistical analysis

Statistical analyses were performed to investigate the differences in the simulated GPP and ET under different hydrological conceptualizations, in both time and space. Simple linear regressions between various scenario estimates (y) and the measured values (x) were made for GPP and ET. Further, Student's t-tests were performed using test-specific hypotheses to ascertain how the slopes of these regressions were statistically different from 1 ($H_0 : \beta_1 = 1$; $H_1 : \beta_1 \neq 1$); how the intercept was different from 0 ($H_0 : \beta_0 = 0$; $H_1 : \beta_0 \neq 0$) and the significance of the regressions ($H_0 : \beta_1 = 0$; $H_1 : \beta_1 \neq 0$) (Montgomery *et al*., 2001). The level of significance for all the tests was fixed at 0·05. In order to test the statistical variability of the scenario performances in time, we used the daily EC-based measurements taken in 2004 ($n = 365$) at the EOBS tower footprint (x) and scenario estimates (y) of ET and GPP to construct the linear regressions. Additionally, root mean square error (RMSE) and the Nash–Sutcliffe efficiency (NSE) were also computed. In order to test the scenario performances in space, 400 randomly distributed sampling points (Figure 1) were identified on the modelling domain using a geographical information system-based approach, after Beyer (2004). A sample size of 400 was adequate to statistically represent a population of size 35 425 pixels at 95% confidence level. The annual values (2004) of the non-explicit (y) and the *Explicit* (x) GPP and ET estimates simulated at these sampling points ($n = 400$) were used to construct the linear regressions for model evaluations.

RESULTS

Temporal dynamics of GPP and ET under various hydrological scenarios

The seasonal patterns of the daily GPP and ET simulated under the three scenarios are shown in the Figure 3. In the model, total GPP is comprised of overstory GPP, understory GPP and moss GPP. In general, the *Implicit* scenario overestimated the daily GPP, whereas the *NoFlow* scenario underestimated daily GPP, in comparison to the *Explicit* scenario and the EC measurements (Figure 3a). The overestimation by the *Implicit* scenario was highest between the days 150 and 200 coinciding with the period of spring snowmelt and soil-water recharge. All the scenarios showed a consistent reduction in the daily GPP between the days 210 and 240, a dry period in 2004. The decline in daily GPP was smaller and slower in

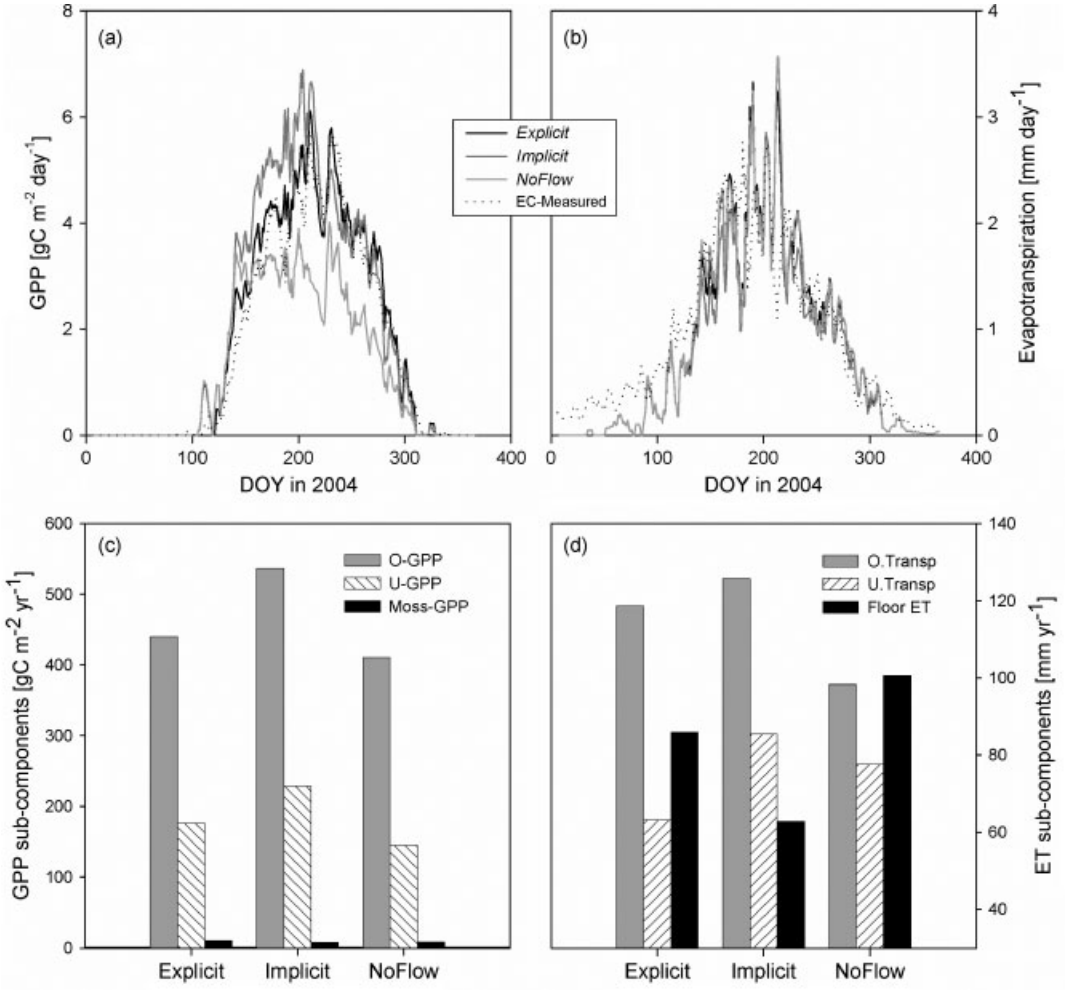

Figure 3. Seasonal dynamics of the simulated (a) GPP and (b) ET vis-à-vis measurements at the EOBS EC-tower footprint region. Relative magnitudes of the annual (c) GPP (d) ET subcomponents simulated under the three scenarios at the EOBS EC-tower footprint region.

DOI: 10.1002/eco

the *NoFlow* scenario, and faster and more pronounced in the *Implicit* scenario than what the *Explicit* scenario simulated.

The temporal pattern of the daily total ET (measurements and simulations) at the EOBS towers footprint region is shown in Figure 3b. In the model, total ET is comprised of overstory transpiration (T_o), understory transpiration (T_{under}), evaporation of intercepted water from the canopy (E_{canopy}) and sublimation of snow (S), and the forest floor evaporation (E_{floor}) comprising of moss evaporation (E_{moss}) and soil evaporation (E_{soil}). Unlike GPP, for daily total ET, all the scenarios showed more or less similar magnitudes. In a strict sense, the *NoFlow* scenario slightly overestimated the daily ET during the spring and in the late summer in comparison to the *Explicit* scenario. Clearly, the subcomponents of ET (both physical and biological) behaved differently under the three scenarios. Although it can be generalized that the simulated ET under the *Implicit* scenario is slightly higher than that of the *Explicit* scenario throughout the year, in the spring the *Implicit* scenario slightly underestimated ET in comparison to the *Explicit* scenario.

The slopes of the linear regressions between the scenario-based daily ET estimates (y) and measured ET estimates (x) at the EOBS tower footprint region revealed that on a daily basis the *NoFlow* scenario slightly underestimated ET, whereas the *Explicit* and the *Implicit* scenarios overestimated ET (Table II). Statistically, the slopes of the linear regressions between *Explicit* ET estimates versus ET measurements (slope = 1·04; $p = 0{\cdot}062$) and the *NoFlow* versus ET measurements (slope = 0·971; $p = 0{\cdot}257$) were not significantly different from 1 (EC measurements). However, the slope of the linear regression between *Implicit* estimates versus EC measurements (slope = 1·052; $p = 0{\cdot}041$)was significantly different from 1, indicating a tendency of the *Implicit* scenario for overestimation. The intercepts in all the scenarios were significantly different from 0 ($p < 0{\cdot}001$). The RMSE was highest for the *NoFlow* scenario (0·447 mm day^{-1}) and lowest for the *Explicit* scenario (0·365 mm day^{-1}) with the *Implicit* scenario having an intermediate level of error (0·418 mm day^{-1}). The NSE was highest for the *Explicit* scenario (0·80) and lowest for the *NoFlow* (0·69) scenario with the *Implicit* scenario having an intermediate level of NSE (0·73).

The slopes of the linear regressions between various scenario-based GPP estimates (y) and measurement-based GPP estimates (x) revealed that on a daily basis the *NoFlow* scenario underestimated GPP, whereas the *Implicit* scenario slightly overestimated GPP relative to the *Explicit* scenario. Statistically, the slope of the linear regression between *Explicit* GPP estimates versus GPP measurements (slope = 1·00; $p = 0{\cdot}991$) was not significantly different from 1, whereas for *NoFlow* estimates versus GPP measurements (slope = 0·64; $p = 0{\cdot}001$) and the *Implicit* estimates versus GPP measurements (slope = 1·09; $p < 0{\cdot}001$), the slopes were significantly different from 1. The RMSE was highest for the *NoFlow* scenario (1·06 gC m^{-2} day^{-1}) and lowest for the *Explicit* scenario (0·50 gC m^{-2} day^{-1}) with the *Implicit* scenario having an intermediate level of accuracy (0·930 gC m^{-2} day^{-1}). The NSE was highest for the *Explicit* scenario (0·91) and lowest for the *NoFlow* (0·58) scenario with the *Implicit* scenario having an intermediate level of NSE (0·76). These results also implied that GPP was more sensitive than ET to the differences in the conceptualization of lateral hydrological processes.

Variation of ET and GPP subcomponents under hydrological scenarios

Ecosystem ET and GPP have various subcomponents representing vegetation (overstory and understory) and forest floor (soil and moss) contributions. We analysed the relative contributions from these subcomponents for

Table II. Statistical measures of model predictability in time.

Scenario	$y = \beta_1 x + \beta_o + \varepsilon$			RMSE[d]	NSE
	Slope (test 1[a])	Intercept (test 2[b])	R^2 (test 3[c])		
$ET_{Explicit}$	1·046 ($p = 0{\cdot}062$)	−0·191 ($p < 0{\cdot}001$)	0·842 ($p < 0{\cdot}001$)	0·365	0·80
$GPP_{Explicit}$	1·001 ($p = 0{\cdot}991$)	0·149 ($p < 0{\cdot}001$)	0·924 ($p < 0{\cdot}001$)	0·500	0·91
$ET_{Implicit}$	1·052 ($p = 0{\cdot}041$)	−0·186 ($p < 0{\cdot}001$)	0·832 ($p < 0{\cdot}001$)	0·418	0·73
$GPP_{Implicit}$	1·087 ($p < 0{\cdot}001$)	0·173 ($p = 0{\cdot}004$)	0·856 ($p < 0{\cdot}001$)	0·930	0·76
ET_{NoFlow}	0·971 ($p = 0{\cdot}257$)	−0·18 ($p < 0{\cdot}001$)	0·804 ($p < 0{\cdot}001$)	0·447	0·69
GPP_{NoFlow}	0·640 ($p = 0{\cdot}001$)	0·194 ($p < 0{\cdot}001$)	0·767 ($p < 0{\cdot}001$)	1·060	0·58

The level of significance of all statistical tests was fixed at 0·05.

[a] Test 1 = $\begin{cases} H_0 : \beta_1 = 1 \\ H_1 : \beta_1 \neq 1 \end{cases}$.

[b] Test 2 = $\begin{cases} H_0 : \beta_0 = 0 \\ H_1 : \beta_0 \neq 0 \end{cases}$.

[c] Test 3 = $\begin{cases} H_0 : \beta_1 = 0 \\ H_1 : \beta_1 \neq 0 \end{cases}$.

$$RMSE = \sqrt{\frac{\sum_{i=1}^{n}(x-y)^2}{n}} \qquad NSE. = \left[1 - \left(\frac{\sum_{i=1}^{n}(x-y)^2}{\sum_{i=1}^{n}(x-\bar{x})^2}\right)\right]$$

[d] RMSE between the measured and simulated ET (mm day^{-1}) and GPP (gC m^{-2} day^{-1}).

DOI: 10.1002/eco

the different scenarios at the EOBS tower footprint region for 2004 (Figure 3c and d).

In all scenarios, for ET, evaporation of the water intercepted by the canopy (E_{canopy}) was simulated to be 58 mm, which was 5·5% of the annual precipitation (1053 mm). This component did not vary in any of the scenario because E_{canopy} was not affected by the nature of soil-water partitioning. Overstory transpiration (T_o) showed pronounced differences among scenarios. In the *Explicit* scenario, T_o was simulated to be 119 mm, in the *Implicit* scenario it increased to 126 mm and in the *NoFlow* scenario it decreased to 98 mm. There were also significant differences in the simulated understory transpiration (T_{under}). It was 63 mm in the *Explicit* scenario, 85 mm in the *Implicit* scenario and 78 mm in the *NoFlow* scenario, showing the high sensitivity of T_{under} to soil moisture fluctuations. As opposed to transpiration components, E_{floor} varied quite differently because of the combined effects of E_{soil} and E_{moss}. E_{floor} was highest in the *NoFlow* scenario (101 mm) and lowest in the *Implicit* scenario (63 mm). Figure 3d shows the relative magnitudes of these ET subcomponents. Simulations also suggested that transpiration was the major contributor to the total ET followed by E_{floor}.

GPP subcomponents also showed pronounced variations under the three scenarios. The footprint-averaged annual overstory GPP (A_o) was simulated to be 440, 536 and 410 gC m^{-2} year^{-1} under the *Explicit, Implicit* and the *NoFlow* scenarios, respectively. The contribution of understory GPP (A_{under}) was 176, 228 and 143 gC m^{-2} year^{-1} for the *Explicit, Implicit* and the *NoFlow* scenarios, respectively. There was a striking reduction in the A_{under} in the *NoFlow* scenario and a drastic increase in the *Implicit* scenario. Moss GPP (A_{moss}) was simulated to be 10·2 gC m^{-2} year^{-1} (*Explicit*), 7·7 gC m^{-2} year^{-1} (*Implicit*) and 8·1 gC m^{-2} yr^{-1}(*NoFlow*) in the three scenarios.

Spatial variability of GPP under hydrological scenarios

After performing the temporal analysis, it was noted that the *Explicit* scenario agreed more closely with the EC measurements than the non-explicit scenarios. Assuming that the *Explicit* scenario was more ideal than the non-explicit scenarios, we did a pixel-to-pixel comparison of the annual GPP simulated at the 400 random sampling points by the two non-explicit scenarios, relative to the *Explicit* scenario (i.e. *Explicit* vs *NoFlow* and *Explicit* vs *Implicit*). This analysis revealed that spatially the simulated GPP varied considerably under the three scenarios. Deviations of the simulated annual GPPs from the 1 : 1 line (Figure 4a) suggested that, in general, the *NoFlow* scenario underestimated GPP. Statistically, the slope of the linear regression between the *Explicit* (x) and the *NoFlow* (y) annual GPPs estimated at the 400 sampling points (slope = 0·820) was significantly different from 1 ($p < 0{\cdot}001$, $n = 400$) and the intercept (−27·32) was significantly different from 0 ($p = 0{\cdot}001$, $n = 400$). Considering all the pixels ($n = 35\,425$ pixels) in the modelling domain, 91% of the *NoFlow* pixels underestimated annual GPP relative to the *Explicit* scenario. It was found that the magnitude of underestimation was as high as −35% of the *Explicit* scenario. There were also few cases of overestimation of the annual GPP as much as +10% of the *Explicit* scenario.

Comparison between the annual GPP estimates between the *Implicit* versus *Explicit* scenarios at the 400 sampling points revealed that the *Implicit* scenario overestimated GPP (positive deviation from the 1 : 1 line; Figure 4a), relative to the *Explicit* scenario. Statistically, the slope of the linear regression between the *Explicit* (x) and the *Implicit* (y) annual GPP estimates (slope = 1·095) was significantly different from 1 ($p < 0{\cdot}001$, $n = 400$) and the intercept (54·75) was

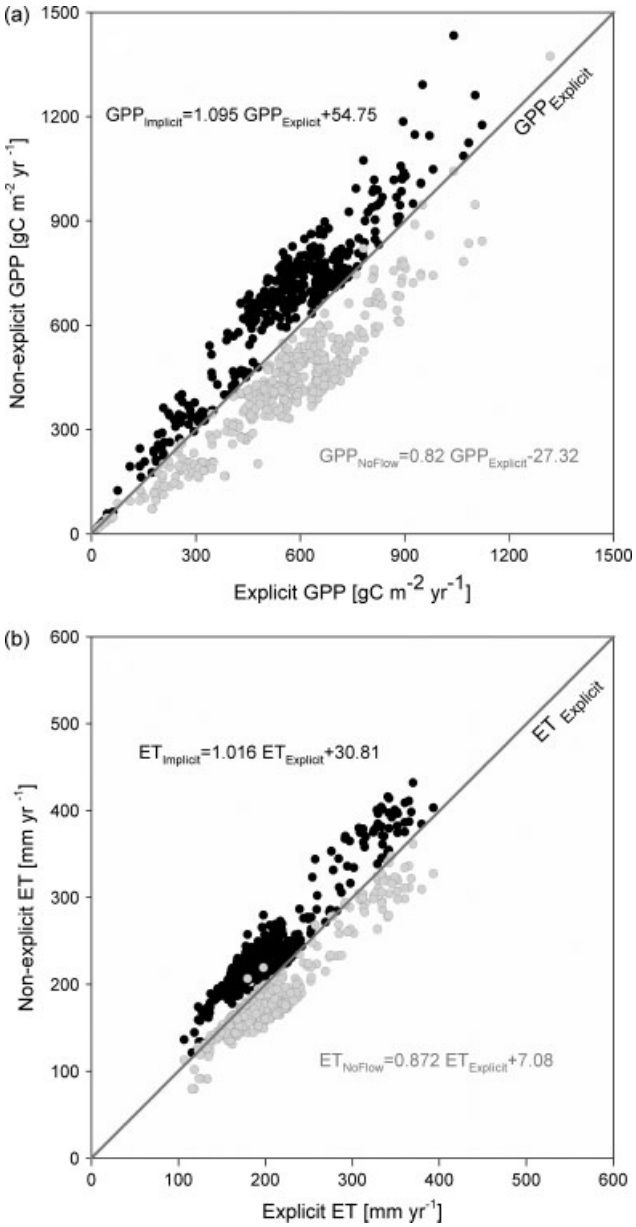

Figure 4. A pixel-to-pixel comparison of (a) annual GPPs at the 400 random sampling points spread across the watershed under the three scenarios. (b) Annual ETs for the 400 random sampling points. Note that the *Explicit* scenario estimates lie in the 1 : 1 line (● *Implicit* estimates; ● *NoFlow* estimates; ━ *Explicit* estimates).

DOI: 10.1002/eco

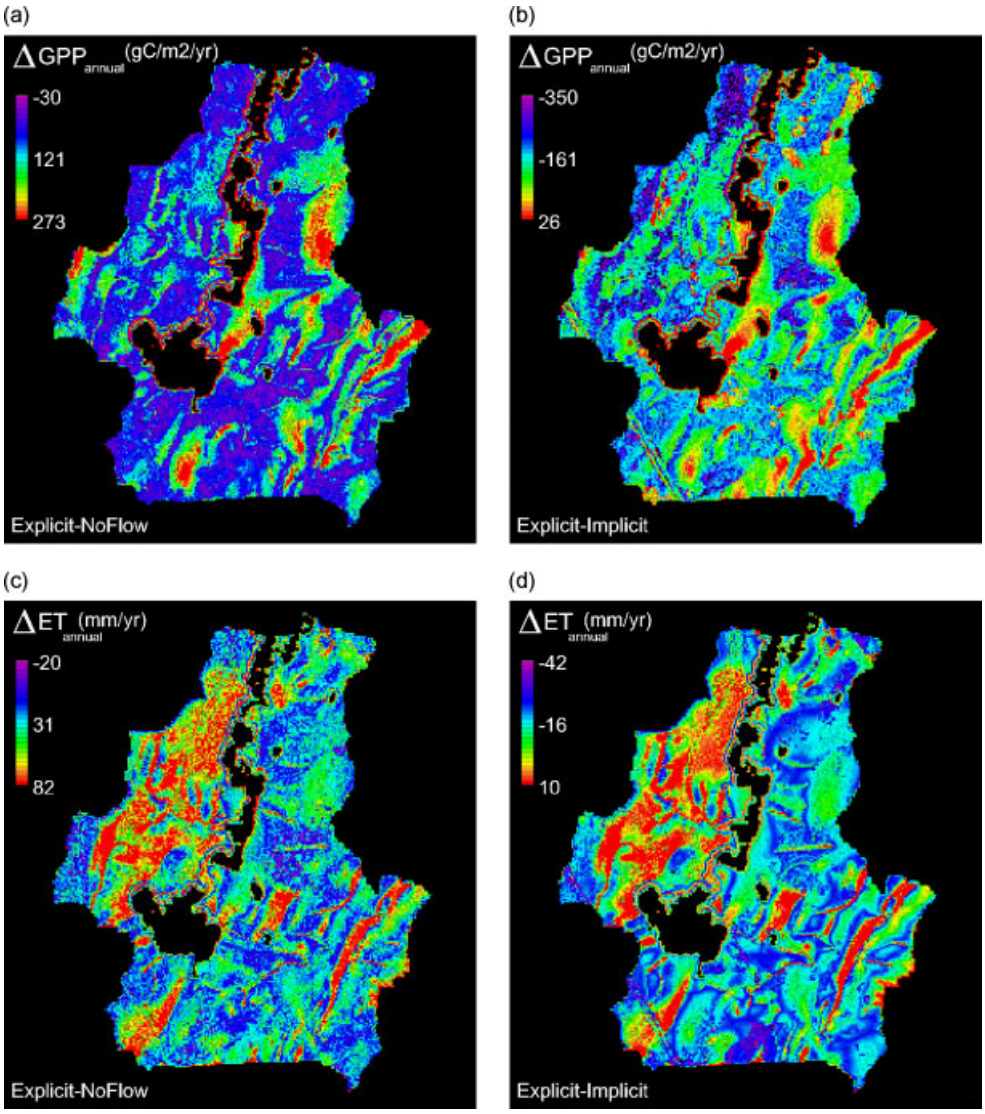

Figure 5. (a) Spatial variability of the GPP difference between the *Explicit* and *NoFlow* scenarios. (b) Spatial variability of the GPP difference between *Implicit and Explicit* scenarios. (c) Spatial variability of the ET difference between the *Explicit* and *NoFlow* scenarios. (d) Spatial variability of the ET difference between *Implicit and Explicit* scenarios.

significantly different from 0 ($p < 0{\cdot}001$, $n = 400$). It was observed that 96% of all the *Implicit* pixels overestimated annual GPP relative to the *Explicit* scenario although a small number of pixels showed underestimation. Although the watershed average GPP bias was as high as $+16{\cdot}4\%$ of the *Explicit* scenario, this bias ranged between $+55\%$ and $-2{\cdot}6\%$. Note that one unit on the x or y axes corresponds to 200 gC m^{-2} $year^{-1}$, which is a substantial amount of C-Flux bias in terms of annual GPP.

Figure 5a shows the spatial differences between the annual GPP simulated using *Explicit* and *NoFlow* scenarios. It can be noted that the differences (underestimations) were greater on the hill-slope locations of the watershed where the influence of SSF was quite high (red tones). On flatter locations, however, the GPP differences (overestimations) were minimal (violet to purple tones). At these locations, because of subtle topographic differences, SSF was not prominent and 'turning-off' SSF did not make much difference to the soil-water status. Consequently, plant physiological conditions were not drastically different in the two scenarios.

In general, in the *Implicit* scenario, the annual GPPs were slightly underestimated on hill-slope locations (Figure 5b, red tones). These trends were observed because SSF fluxes were suppressed consequent of ignoring topographic controls on SSF calculation. However, this scenario greatly overestimated annual GPP on flatter locations (blue tones) because it unrealistically maintained the hyperoptimal soil moisture conditions that facilitated increased photosynthesis because of excessive SSF. Locations that were dominated by deciduous species showed a striking overestimation of the annual GPP. For example, in the northwestern parts of the watershed where mixed forests are found on the esker ridges, there was a significant overestimation of annual GPP (as much as -341 gC m^{-2} $year^{-1}$). On hill-slope locations (red tones), however, the annual GPPs were only slightly underestimated (e.g. $+26$ gC m^{-2} $year^{-1}$ in Figure 5b) because the implicitly simulated SSF fluxes were less

DOI: 10.1002/eco

than 'ideal' (i.e. *Explicit*) and this lead to conditions of slight soil saturation resulting in only a smaller reduction in photosynthesis. Thus, implicit conceptualization of lateral hydrological processes had a general tendency to overestimate photosynthesis.

From these results, it can be deduced that positive GPP biases created due to the *Implicit* scenario are more intense on flat areas than on hill-slope locations. For the *NoFlow* scenario, however, negative GPP biases are more intense on the hill-slope locations than flat areas. We speculate that factors such as soil hydraulic properties (e.g. Ksat, field capacity, wilting point), the nature of the vegetation and the mechanisms of biogeochemical cycling (soil C-pool dynamics and consequent N release) interactively govern the hydroecological response within a given topographic location.

Spatial variability of ET under various scenarios

A pixel-to-pixel comparison of the simulated annual ET under the *Explicit* and the *NoFlow* scenarios at the 400 sampling points revealed that the *NoFlow* scenario slightly underestimated the annual ET relative to the *Explicit* scenario (Figure 4b). Statistically, the slope of the linear regression between the *Explicit* (x) and the *NoFlow* (y) annual ET estimates (0·87) was significantly different from 1 ($p < 0{\cdot}001$, $n = 400$) and the intercept (7·08) was significantly different from 0 ($p = 0{\cdot}016$, $n = 400$), revealing that although underestimation was slight, it was statistically significant. Considering all the pixels ($n = 35\,425$ pixels) in the modelling domain, it was found that 81% of the *NoFlow* pixels underestimated annual ET relative to the *Explicit* scenario. The magnitudes of biases ranged between +15% and −8·1%, and on an average the underestimation was around −1·8% of the *Explicit* scenario which indicated that some form of compensatory mechanism was associated with ET subcomponents under varying soil hydrological conditions.

The spatial distributions of the differences in the annual ET under the *NoFlow* and the *Implicit* scenarios are shown in the Figures 5c and 5d, respectively. In general, the *NoFlow* scenario underestimated (positive values) annual ET relative to the *Explicit* scenario (locations having cyan to red tones). The most prominent underestimations were seen on the northwestern parts and in the low-lying locations of the watershed. The northwestern locations represent mesoscale topographic features that were formed due to glacial activities, e.g. drumlins or eskers where ridges and depressions exist in parallel. These depressions accumulated water from the nearby ridges and hence the major contributor of the total annual ET in these locations was E_{floor}. Under the *NoFlow* scenario, these locations dried out due to the absence of SSF contributions from surrounding regions (a 'decoupling effect') and total annual ET was reduced due to suppressed E_{floor}. A similar situation existed in the depressions located in the southern part of the watershed, near streams and rivulets.

Comparison of the simulated annual ETs between the *Implicit* and the *Explicit* scenarios revealed that the *Implicit* scenario showed overestimation (Figure 4b). However, in this case the slope of the linear regression (1·016) was not significantly different from 1 ($p = 0{\cdot}383$, $n = 400$) although the intercept (30·81) was significantly different from 0 ($p < 0{\cdot}001$, $n = 400$). Considering all the pixels ($n = 35\,425$ pixels) in the modelling domain, it was found that 92% of the *Implicit* pixels overestimated annual ET relative to the *Explicit* scenario. The magnitudes of positive biases were much higher than that of negative biases. Although these biases ranged between +16·4% and −12·8%, on an average, the overestimation was +3·5% relative to the *Explicit* scenario.

In general, the *Implicit* scenario (Figure 5d) overestimated the annual ET on flatter locations of the watershed (locations having bluish tones). However, at locations with depressions (in the northwestern part) and rivulets (southeastern part), the overestimations were weaker (yellow to orange tones). The soils at these locations were simulated to be 'drier than usual' because of the combined effects of excessive SSF fluxes and the absence of influx of water from the surrounding areas ('a decoupling effect' analogous to what Devito *et al.* (2005) observed during dry periods in a similar environment). This decoupling effect resulted in decreased soil moisture that consequently lowered the E_{floor} although the transpiration components slightly increased. This condition resulted only in a very small increase in total annual ET (locations having dark red tones).

From the magnitudes of the differences in the simulated ecophysiological processes under different scenarios and from the magnitudes of the RMSEs shown in Table III, we can deduce that photosynthesis is more sensitive to lateral hydrological representations than ET.

DISCUSSION

Effects of lateral hydrological processes on soil-water balance

On an annual basis, the partitioning of the annual infiltrated soil water (I) in the three scenarios were different. The nature of soil hydrological processes had considerable effects on the corresponding rhizosphere moisture regimes that consequently affected GPP and ET via physiological variations in the canopy. The trends in the nature of soil-water balance affected the dynamics of the simulated WTD. Figure 6a shows the WTD simulated by the three scenarios for the pixel that includes the location where piezometer readings were taken at the EOBS site in 2004. At the EOBS tower footprint region, in the *Explicit* scenario, which simulated the ecophysiological processes most ideally, the main mechanism of soil-water partitioning was via SSF (64% of I) followed by ET (27% of I). The remainder of the water (0·5% of I) was used to slightly increase the soil storage during the 1-year time period. Under the *NoFlow* scenario, where the SSF was 'turned-off', the main mechanism of soil-water partitioning was via SOLF

DOI: 10.1002/eco

Table III. Statistical measures of model predictability in space.

Scenario	$y = \beta_1 x + \beta_o + \varepsilon$			RMSE[d]
	Slope (test 1[a])	Intercept (test 2[b])	R^2 (test 3[c])	
$ET_{Implicit}$	1·016 ($p = 0·383$)	30·81 ($p < 0·001$)	0·88 ($p < 0·001$)	40·0
$GPP_{Implicit}$	1·095 ($p < 0·001$)	54·75 ($p < 0·001$)	0·92 ($p < 0·001$)	129·2
ET_{NoFlow}	0·872 ($p < 0·001$)	7·08 ($p = 0·016$)	0·91 ($p < 0·001$)	26·0
GPP_{NoFlow}	0·82 ($p < 0·001$)	−27·32 ($p = 0·001$)	0·89 ($p < 0·001$)	144·5

y = Non-explicit scenario estimate; x = *Explicit* scenario estimate; n = 400 random points in the watershed. The level of significance of all statistical tests was fixed at 0·05.

[a] Test 1 = $\begin{cases} H_0 : \beta_1 = 1 \\ H_1 : \beta_1 \neq 1 \end{cases}$.

[b] Test 2 = $\begin{cases} H_0 : \beta_0 = 0 \\ H_1 : \beta_0 \neq 0 \end{cases}$.

[c] Test 3 = $\begin{cases} H_0 : \beta_1 = 0 \\ H_1 : \beta_1 \neq 0 \end{cases}$.

[d] RMSE between the *Explicit* and non-explicit ET (mm year^{-1}) and GPP (gC m^{-2} year^{-1}).

(66% of I), followed by ET (24·5% of I). Under this scenario, SOLF occurred only after the soil profile was saturated up to the soil surface (i.e. WTD = 0) and only the excess water that was ponded on the soil surface was subjected to lateral flow. Because of this, there was a large increase in the soil storage (9·6% of I) on an annual basis. On the other hand, in the *Implicit* scenario, the SSF was 76·2% of I. This increase in SSF occurred because it was assumed that the amount of water that exceeded the field capacity in the saturated zone was lost via SSF consequently reducing the soil storage (8·6% of I) over the year.

Under the *NoFlow* scenario, increased wetting of the soil profile caused a large fraction of the soil profile to remain in the saturated condition (where the VSMC = θ_s) for most parts of the year. However, in the *Implicit* scenario, a large fraction of the soil profile remained in the unsaturated condition where the VSMC remained between the field capacity and the permanent wilting point for most parts of the year. Apart from SSF, ET also played a critical role in modulating the soil-water balance. In all the three scenarios, ET was calculated as the sum of several subcomponents. In general, the transpiration subcomponents declined under the *NoFlow* scenario, while the E_{floor} increased where the soil profile mostly remained in the saturated condition (Figure 3). For those locations that usually receive water from uphill locations, ET reduced because of a consequent reduction in E_{floor} owing to soil drying. However for the *Implicit* scenario, in general, the transpiration subcomponents increased although E_{floor} declined because the soil became drier.

Although we conducted the analysis only for a single year (2004), we believe that similar ecohydrological interactions are plausible even if interannual variability in P is taken into account. In this excessively humid ecosystem, where the annual ET is much lower than annual P (see the online Supporting Information), interannual variabilities in P are still able to result in considerable amount of soil water that is fluxed as SSF. Therefore, we believe that similar effects are plausible, although with different magnitudes. However, in water-limited ecosystems, the influence of interannual variability may be critical in deciding the direction and magnitudes of these ecohydrological interactions.

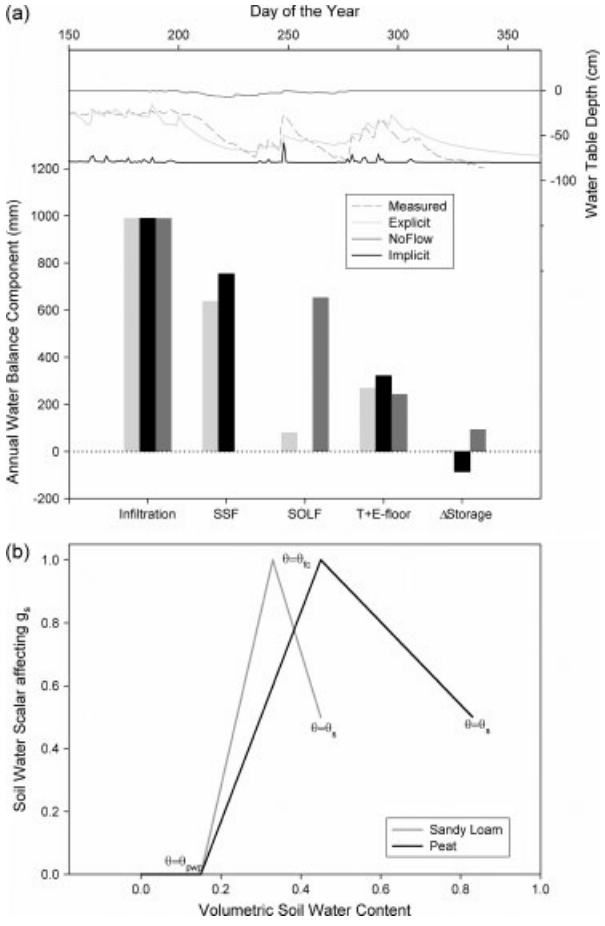

Figure 6. (a) Nature of water balance at the EOBS tower footprint region in 2004, vis-à-vis the nature of the simulated WTDs under various hydrological scenarios. (b) Nature of the soil-water scalar for a wide range of soil moisture conditions, for different soil texture types. This scalar is used to constrain the maximum stomatal conductance, $g_{s,max}$.

Effects of lateral hydrological processes on plant physiological status

While total runoff (SOLF + SSF) was comparable in all the three scenarios, the nature of their soil-water partitioning was different. The differences in the simulated

DOI: 10.1002/eco

GPP and ET under the three scenarios can be attributed mainly due to differences in the plant physiological statuses consequent of the soil-water conditions.

The ambient g_s is an important ecophysiological factor which is governed by several environmental variables. Soil-water status is one of the most influential and dynamic factor that controls g_s (Chen *et al*., 2005; Sonnentag *et al*., 2008). Hydrological controls on photosynthesis are manifested through deficits or excesses of soil water (Kozlowski, 2000; Zgallai *et al*., 2006; Galmes *et al*., 2007). Although there are many explanations regarding the physiological mechanism regarding the control of soil water on primary production, the most accepted is that of Schulze *et al*. (1994) who hypothesized that a phytohormone (abscisic acid) produced by stressed root tips when transported through xylem makes the leaves to close stomata and reduce transpiration losses. Nevertheless, $g_{s,max}$ can vary widely among and within species (Kelliher *et al*., 1995; Dang *et al*., 1997, 1998) and hence the magnitudes of g_s increases with $g_{s,max}$ (Landsberg and Waring, 1997; Arain *et al*., 2002). For example, g_s of a healthy black spruce leaf may be similar to the g_s of a deciduous species under stress. In the Jarvis (1976) algorithm, the soil-water scalar $f(\theta)$ that governs ambient g_s is a function of VSMC. It is important to note that in BEPS-TerrainLab V2.0, although the value of this scalar linearly increases between the permanent wilting point and the field capacity, when VSMC increases beyond the field capacity, its value decreases (Figure 6b). On the other hand, moss conductance (g_{moss}) and soil-surface conductance (g_{soil}) increases with an increase in VSMC. This is the reason for increased E_{floor} under the *NoFlow* scenario (where the soil is generally wet) and vice versa in the *Implicit* scenario.

In general, the g_s simulated by the *NoFlow* scenario was lower than that of the *Explicit* scenario, while the *Implicit* scenario had higher values (Figure 7a). The differences were large in the spring when the SSF fluxes intensified because of the wetting of soil profile due to snow melt water. In the *NoFlow* scenario, in general, since the soil remained saturated spatially and temporally, g_s remained lower relative to the *Explicit* scenario, which consequently decreased the transpiration and photosynthesis. The decrease in transpiration components created a positive feedback loop which further maintained the VSMC without much alteration triggering a further reduction of transpiration and photosynthesis. However, the total ET was not greatly affected because soil and moss surface conductances increased which resulted in an increase in E_{floor}. Nevertheless, the sum of transpiration and E_{floor} (24·5% of infiltrated water) remained slightly lower than what was in the *Explicit* scenario.

Because the *Implicit* scenario simulated SSF with no topographical controls, soil water that had energy status above the field capacity was allowed to 'drain-off' which resulted in well-drained conditions even in flatter locations. The soil profile remained unsaturated for most parts of the year and unrealistically created optimal

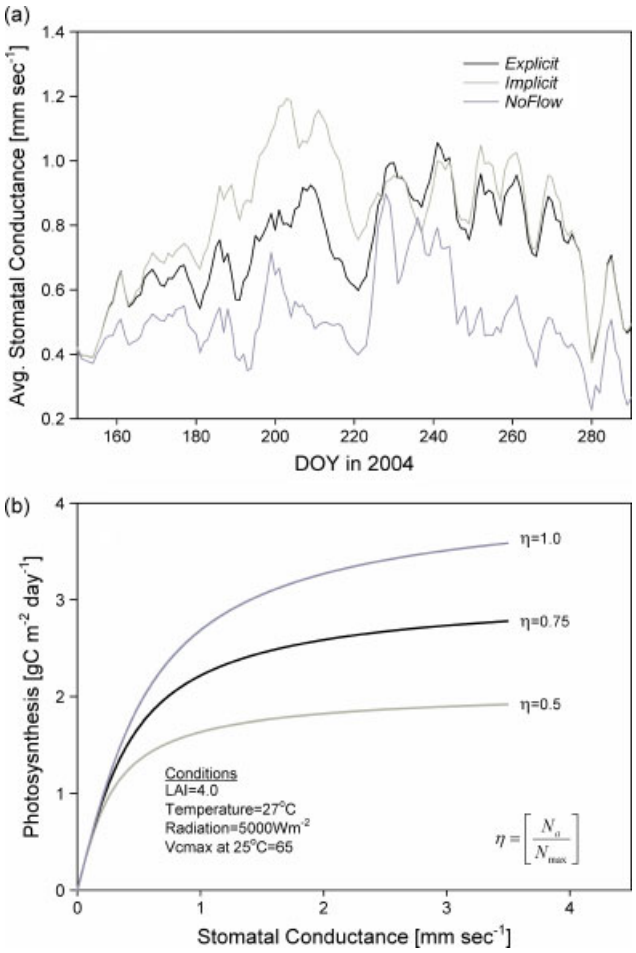

Figure 7. (a) Seasonal dynamics of the average g_s in the footprint region, under different scenarios. Note the pronounced underestimation by the *NoFlow* scenario and overestimation by the *Implicit* scenario in comparison to the *Explicit* scenario. (b) Relationship between g_s and GPP at various levels of leaf N, for a given set of conditions. Both g_s and leaf N are hydrologically controlled creating a positive feedback mechanism within the model.

conditions (given the fact that this is a humid ecosystem) and increased g_s. This resulted in an increase in the transpiration components although the E_{floor} reduced. Nevertheless, the sum of transpiration and E_{floor} remained higher than that of the *Explicit* scenario because transpiration was the largest contributor to the total ET. Similar to transpiration, photosynthesis also altered under the influence of g_s.

Soil profile generally remained saturated under the *NoFlow* scenario. Consequently, WTD mostly remained near the soil surface which created optimal conditions for increased E_{floor} due to increased g_{soil} and g_{moss}. This compensated for the reduction in the transpiration components in the total ET. Due to this compensatory mechanism, total ET simulated under the *NoFlow* scenario was only slightly lower in comparison to the *Explicit* scenario. Sonnentag *et al*. (2008) working on a peat land ecosystem also reported that ET was less sensitive than GPP under differences in soil moisture status. Under the *Implicit* scenario, however, the annual total ET generally increased due to enhanced plant transpiration although E_{floor} declined.

DOI: 10.1002/eco

Effects of lateral hydrological processes on nutrient dynamics

Hydrologically controlled nutrient, (N) dynamics also contributed to the biases in the simulated GPP in addition to g_s. Differences in hydrological regimes can alter the local-scale biogeochemical processes which indirectly regulate photosynthesis through N availability. For example, in BEPS-TerrainLab V2.0, leaf N status affects the rate of rubisco activity and therefore photosynthesis. A detailed analysis of hydrologically controlled biogeochemical processes through the dynamics of various soil C-pools and N-mineralization is beyond the scope of this article and is exclusively addressed in Govind *et al*. (2009b). It was shown that under the non-explicit scenarios, N-mineralization altered, consequent of variability in soil hydrothermal conditions. Leaf N concentration directly affects photosynthesis by altering the V_{cmax} (Dang *et al*., 1997), the maximum carboxylation rate in the TIFM of Chen *et al*. (1999), used within BEPS-TerrainLab V2.0.

While hydrologically controlled ecophysiological processes are mainly governed by the stomatal dynamics, a synergism between g_s and N status makes the system more nonlinear. Conceptually, the interaction between g_s, N status and photosynthesis operating within BEPS-TerrainLab V2.0 is shown in the Figure 7b. This relationship is plotted based on a set of hypothetical conditions with only g_s and N as variables. Note the close interaction between g_s and plant N status in affecting photosynthesis. This synergism might be the reason for the drastic overestimation of GPP under the *Implicit* scenario, especially for deciduous and mixed-forest stands, where hyperoptimal VSMC favours N-mineralization.

Effects of lateral hydrological processes on rhizosphere wetting patterns that govern ecophysiological processes

Differences in the input and output components of soil-water balance result in variations in the soil-water storages under the three scenarios. Conceptually, in BEPS-TerrainLab V2.0, the soil storage consists of unsaturated and saturated zones, whose depths are determined by WTD. In the unsaturated zone, VSMC $= \theta$ and in the saturated zone, because all soil pores are filled with water, VSMC $= \theta_s = \phi$. Different hydrological scenarios resulted in unique combinations of saturated and unsaturated zones in the soil which affected the rhizosphere wetting patterns. In the model, the rhizosphere wetting pattern is modelled as a function of root geometry and the WTD according to Gale and Grigal (1987). This method calculates the fractions of roots lying in the unsaturated (μ) and saturated zones ($1 - \mu$). Figure 8a shows how the model captures the relative variations in μ and $(1 - \mu)$ as a function of WTD for different types of root geometries. Species-specific root geometries are quantified by the root extinction coefficient (ρ), after Jackson *et al*. (1996). As the water table rises (i.e. WTD decreases), μ decreases, whereas $(1 - \mu)$ increases. For shallow-rooted plants such as understory shrubs (e.g. $\rho = 0{\cdot}88$), μ rapidly reaches 100% for a WTD as shallow as 35 cm, and for deep-rooted plants (e.g. $\rho = 0{\cdot}945$), μ reaches 100% only when WTD is as deep as 80 cm. Because the understory roots are shallower than the overstory roots, they are more sensitive to alterations in the rhizosphere wetting patterns. This was the reason for larger variability in the understory transpiration components under the three scenarios as shown in Figure 3. In the model, rhizosphere wetting patterns have major implications on the spatial upscaling of leaf-scale ecophysiological processes as described in Equations (3) and (5).

It is assumed that the differences in root wetting patterns proportionately influence the physiological statuses of the leafs in the canopy, analogous to the pipe theory (Shinozaki *et al*., 1964). Because the rhizosphere wetting patterns differed in the three scenarios, the magnitudes of ecophysiological processes they simulated also varied. For example, in the *NoFlow* scenario, since the soil profile becomes excessively saturated, μ declined and $(1 - \mu)$ increased. On the other hand, under the *Implicit* scenario, the opposite is true, i.e. μ increases (Figure 8c). It has to be recollected that in this humid ecosystem, g_s for the leafs corresponding to saturated soil moisture regime (VSMC $= \theta_s = \phi$) is substantially lower than those leafs corresponding to unsaturated soil moisture regime (VSMC $= \theta$).

The scenarios showed differences in simulated ecophysiological processes consequent of the rhizosphere wetting patterns mainly due to the changes in the magnitudes of μ and $1 - \mu$ which are the weighting terms that upscale leaf-level processes to the canopy. This implies that parameterization of root distributions could have implications on the ecohydrological simulations. Figure 8b implies that in general increasing ρ values could lead to decreasing μ biases (and vice versa) which cascades into ecohydrological biases via Equations (3) and (5). It also has to be noted that these biases occur nonlinearly depending on the position of the WTD. At shallower WTDs, effects of ρ parameter errors are more significant than at deeper WTDs implying the higher vulnerability of the *NoFlow* in comparison to the *Implicit* scenario for errors in ρ parameterization.

SUMMARY AND CONCLUSIONS

There is a growing interest in comprehending the relationships between hydrological and ecological processes. To advance our understanding of terrestrial biogeochemical processes in conjunction with climate change, coupled representations of hydrological and ecophysiological processes within models are necessary. In this context, we carried out a modelling experiment to demonstrate the importance of explicitly incorporating hydrological processes within ecological models. Based on the results of our numerical experiment, we draw the following conclusions:

1. In humid ecosystems, an ecological model that ignores SSF underestimates the simulated ET and GPP in

DOI: 10.1002/eco

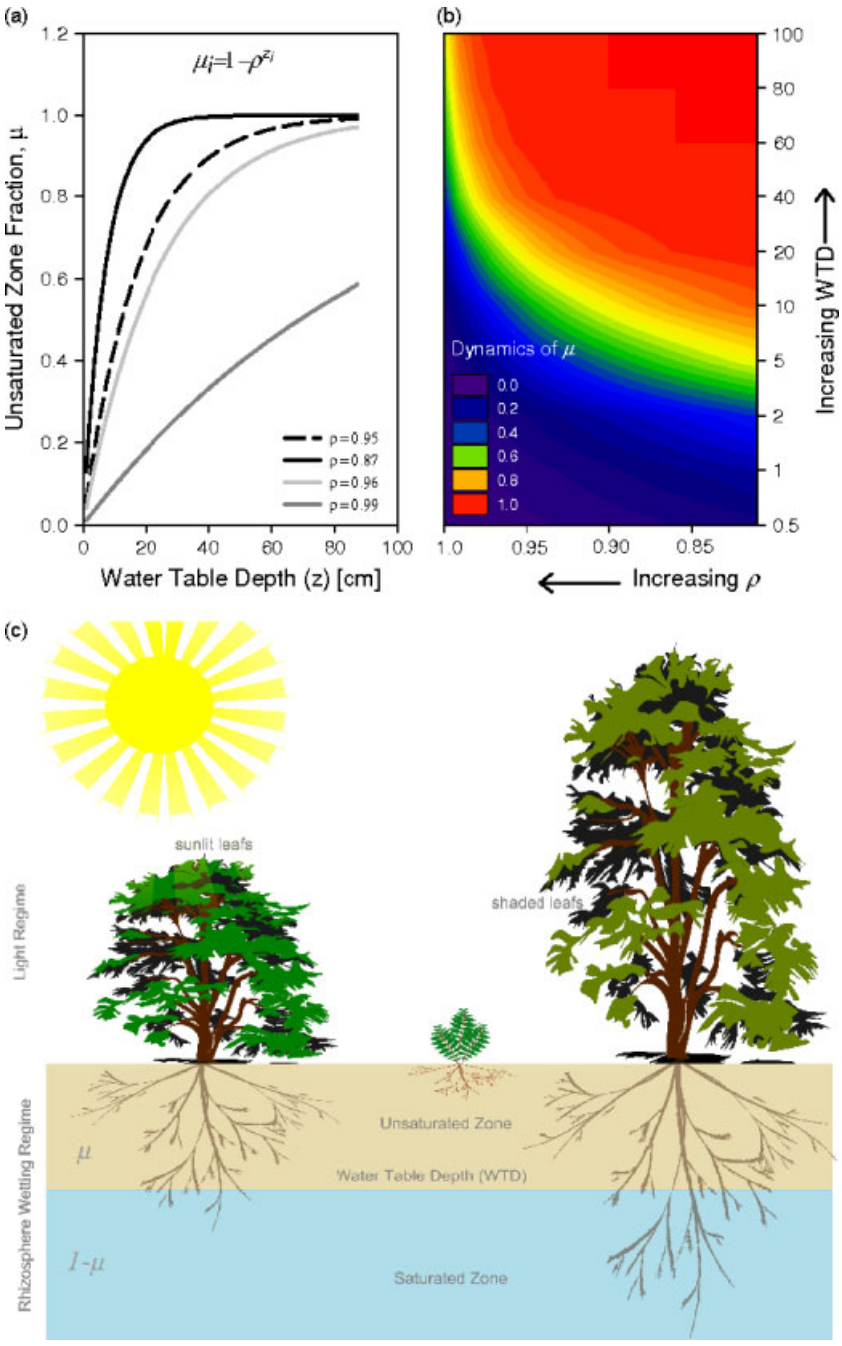

Figure 8. (a) Partitioning of the unsaturated (μ) and saturated ($1 - \mu$) root fractions as a function of water table position (z cm from the surface) and the root decay constant (ρ), a land cover-specific parameter describing the root geometry. (b) Sensitivity of ρ in conjunction with WTD towards rhizophere wetting patterns (c) A schematic representation of the variability in resources (light and water) that create physiological variability in the modelling domain. Note the separation of roots into unsaturated and saturated fractions as a function of root geometry factor, ρ, and water table, z.

comparison to the reality. On the other hand, an ecological model having a simplified 'bucket-like' hydrological representation overestimates GPP and ET. These biases (in space and time) are created due to alterations in plant physiological status, nutrient dynamics and feedback relationships consequent of soil-water status, depending on the differences in the conceptualization of lateral hydrological processes.

2. Although both ET and GPP are sensitive to soil hydrological regimes, ET biases are not as prominent as GPP biases. This is because ET subcomponent processes behave differently with compensatory mechanisms as opposed to GPP subcomponents.

Until now, ecological modellers (mostly biologists) and hydrological modellers (mostly civil engineers) worked in isolation. Even though this resulted in parallel advancements in both the fields, these scientific communities have overlooked the capabilities that the combination of hydrology and ecology can bring to a better understanding of earth surface processes. In order to accurately represent hydrological controls on biogeochemical processes within ecological models, the currently existing

DOI: 10.1002/eco

simplified hydrological conceptualizations need to be changed. Although the study was conducted in a humid boreal ecosystem, we hope that these findings will speak to similar issues in other ecohydrological environments where water-mediated fluxes of mass and energy are crucial.

ACKNOWLEDGEMENTS

This work was supported by the CCP, funded by the Canadian Foundation for Climate and Atmospheric Sciences (CFCAS), Natural Sciences and Engineering Research Council of Canada (NSERC) and BIOCAP Canada. We thank Hank Margolis, P.I. CCP and the site-PI of EOBS site. We thank the anonymous reviewers whose suggestions greatly improved the manuscript.

REFERENCES

Arain MA, Black TA, Barr AG, Jarvis PG, Massheder JM, Verseghy DL, Nesic Z. 2002. Effects of seasonal and interannual climate variability on net ecosystem productivity of boreal deciduous and conifer forests. *Canadian Journal of Forest Research-Revue Canadienne De Recherche Forestiere* **32**: 878–891.

Arain MA, Yuan FM, Black TA. 2006. Soil-Plant Nitrogen Cycling Modulated Carbon Exchanges in a Western Temperate Conifer Forest in Canada. *Agricultural and Forest Meteorology* **140**: 171–192.

Armstrong RN, Martz LW. 2003. Topographic parameterization in continental hydrology: a study in scale. *Hydrological Processes* **17**: 3763–3781.

Arora VK, Boer GJ. 2006. The temporal variability of soil moisture and surface hydrological quantities in a climate model. *Journal of Climate* **19**: 5875–5888.

Barr AG, Black TA, Hogg EH, Kljun N, Morgenstern K, Nesic Z. 2004. Inter-annual variability in the leaf area index of a boreal aspen-hazelnut forest in relation to net ecosystem production. *Agricultural and Forest Meteorology* **126**: 237–255.

Bergeron O, Margolis HA, Black TA, Coursolle C, Dunn AL, Barr AG, Wofsy SC. 2007. Comparison of carbon dioxide fluxes over three boreal black spruce forests in Canada. *Global Change Biology* **13**: 89–107.

Bergeron O, Margolis H, Coursolle C, Giasson MA. 2008. How does forest harvest influence carbon dioxide and water fluxes of black spruce ecosystems in eastern North America?. *Agricultual and Forest Meteorology* (in press).

Beven KJ, Kirkby MJ, Schofield N, Tagg AF. 1984. Testing a physically-based flood forecasting-model (Topmodel) for 3 Uk catchments. *Journal of Hydrology* **69**: 119–143.

Beyer HL. 2004. Hawth's analysis tools for ArcGIS. Available at http://www.spatialecology.com/htools..

Chen JM, Liu J, Cihlar J, Goulden ML. 1999. Daily canopy photosynthesis model through temporal and spatial scaling for remote sensing applications. *Ecological Modelling* **124**: 99–119.

Chen JM, Ju WM, Cihlar J, Price D, Liu J, Chen WJ, Pan JJ, Black A, Barr A. 2003. Spatial distribution of carbon sources and sinks in Canada's forests. *Tellus Series B-Chemical and Physical Meteorology* **55**: 622–641.

Chen JM, Chen XY, Ju WM, Geng XY. 2005. Distributed hydrological model for mapping evapotranspiration using remote sensing inputs. *Journal of Hydrology* **305**: 15–39.

Comer NT, Lafleur PM, Roulet NT, Letts MG, Skarupa M, Verseghy D. 2000. A test of the Canadian Land Surface Scheme (CLASS) for a variety of wetland types. *Atmosphere-Ocean* **38**: 161–179.

Coops NC, Black TA, Jassal RPS, Trofymow JAT, Morgenstern K. 2007. Comparison of Modis, eddy covariance determined and physiologically modelled gross primary production (Gpp) in a Douglas-fir forest stand. *Remote Sensing of Environment* **107**: 385–401.

Cox PM, Betts RA, Bunton CB, Essery RLH, Rowntree PR, Smith J. 1999. The impact of new land surface physics on the GCM simulation of climate and climate sensitivity. *Climate Dynamics* **15**: 183–203.

Daly E, Porporato A, Rodriguez-Iturbe I. 2004. Coupled Dynamics of photosynthesis, transpiration, and soil water balance. Part I: upscaling from hourly to daily level. *Journal of Hydrometeorology* **5**: 546–558.

DangQL, MargolisHA, CoyeaMR, SyM, Collatz GJ. 1997. Regulation of branch-level gas exchange of boreal trees: roles of shoot water potential and vapor pressure difference. *Tree Physiology* **17**: 521–535.

Dang QL, Margolis HA, Collatz GJ. 1998. Parameterization and testing of a coupled photosynthesis stomatal conductance model for boreal trees. *Tree Physiology* **18**: 141–153.

Devito KJ, Creed IF, Fraser CJD. 2005. Controls on runoff from a partially harvested aspen-forested headwater catchment, boreal plain, Canada. *Hydrological Processes* **19**: 3–25.

Dunne T, Black RD. 1970. Partial area contributions to storm runoff in a small New England watershed. *Water Resources Research* **6**: 1296–1311.

Else MA, Tiekstra AE, Croker SJ, Davies WJ, Jackson MB. 1996. Stomatal closure in flooded tomato plants involves abscisic acid and a chemically unidentified antitranspirant in xylem sap. *Plant Physiology* **112**: 239–247.

Environment Canada. 2006. Canadian climate normals or averages 1971–2000. http://www.climate.weatheroffice.ec.gc.ca/climate_normals/index_1961_1990_e.html.

Gale MR, Grigal DF. 1987. Vertical root distributions of northern tree species in relation to successional status. *Canadian Journal of Forest Research-Revue Canadienne De Recherche Forestiere* **17**: 829–834.

Galmes J, Flexas J, Save R, Medrano H. 2007. Water relations and stomatal characteristics of Mediterranean plants with different growth forms and leaf habits: responses to water stress and recovery. *Plant and Soil* **290**: 139–155.

Gedney N, Cox PM, Betts RA, Boucher O, Huntingford C, Stott PA. 2006. Detection of a direct carbon dioxide effect in continental river runoff records. *Nature* **439**: 835–838.

Giasson MA, Coursolle C, Margolis HA. 2006. Ecosystem-level Co2 fluxes from a boreal cutover in eastern Canada before and after scarification. *Agricultural and Forest Meteorology* **140**: 23–40.

Govind A, Chen JM, Margolis H, Ju W, Sonnentag O, Giasson MA. 2009a. A spatially explicit hydro-ecological modeling framework (BEPS-TerrainLab V2.0): model description and test in a boreal ecosystem in eastern North America. *Journal of Hydrology* **367**: 200–216.

Govind A, Chen JM, Ju W. 2009b. Spatially explicit simulation of hydrologically controlled carbon and nitrogen cycles and associated feedback mechanisms in a boreal ecosystem. *Journal of Geophysical Research* **114**: G02006, DOI: 10.1029/2008JG000728.

Grant RF, Zhang Y, Yuan F, Wang S, Hanson PJ, Gaumont-Guay D, Chen J, Black TA, Barr A, Baldocchi DD, Arain A. 2006. Intercomparison of techniques to model water stress effects on Co2 and energy exchange in temperate and boreal deciduous forests. *Ecological Modelling* **196**: 289–312.

Heinsch FA, Zhao MS, Running SW, Kimball JS, Nemani RR, Davis KJ, Bolstad PV, Cook BD, Desai AR, Ricciuto DM, Law BE, Oechel WC, Kwon H, Luo HY, Wofsy SC, Dunn AL, Munger JW, Baldocchi DD, Xu LK, Hollinger DY, Richardson AD, Stoy PC, Siqueira MBS, Monson RK, Burns SP, Flanagan LB. 2006. Evaluation of remote sensing based terrestrial productivity from Modis using regional tower eddy flux network observations. *Ieee Transactions on Geoscience and Remote Sensing* **44**: 1908–1925.

Horton RE. 1933. The role of infiltration in the hydrological cycle. *Transactions: American Geophysical Union* **14**: 446–460.

Jackson RB, Canadell J, Ehleringer JR, Mooney HA, Sala OE, Schulze ED. 1996. A global analysis of root distributions for terrestrial biomes. *Oecologia* **108**: 389–411.

Jarvis PG. 1976. Interpretation of variations in leaf water potential and stomatal conductance found in canopies in field. *Philosophical Transactions of the Royal Society of London Series B-Biological Sciences* **273**: 593–610.

Joos F, Prentice IC, Sitch S, Meyer R, Hooss G, Plattner GK, Gerber S, Hasselmann K. 2001. Global warming feedbacks on terrestrial carbon uptake under the Intergovernmental Panel on Climate Change (IPCC) emission scenarios. *Global Biogeochemical Cycles* **15**: 891–907.

Ju WM, Chen JM, Black TA, Barr AG, Mccaughey H, Roulet NT. 2006. Hydrological effects on carbon cycles of Canada's forests and wetlands. *Tellus Series B-Chemical and Physical Meteorology* **58**: 16–30.

Kelliher FM, Leuning R, Raupach MR, Schulze ED. 1995. Maximum conductances for evaporation from global vegetation types. *Agricultural and Forest Meteorology* **73**: 1–16.

Koster RD, Guo ZC, Dirmeyer PA, Bonan G, Chan E, Cox P, Davies H, Gordon CT, Kanae S, Kowalczyk E, Lawrence D, Liu P, Lu CH,

Malyshev S, Mcavaney B, Mitchell K, Mocko D, Oki T, Oleson KW, Pitman A, Sud YC, Taylor CM, Verseghy D, Vasic R, Xue YK, Yamada T. 2006. Glace: the Global land-atmosphere coupling experiment. Part I: overview. *Journal of Hydrometeorology* **7**: 590–610.

Kozlowski TT. 1984. *Flooding and Plant Growth*. Academic Press: New York; 356.

Kozlowski TT. 2000. Responses of woody plants to human-induced environmental stresses: issues, problems, and strategies for alleviating stress. *Critical Reviews in Plant Sciences* **19**: 91–170.

Landsberg JJ, Waring RH. 1997. A generalised model of forest productivity using simplified concepts of radiation-use efficiency, carbon balance and partitioning. *Forest Ecology and Management* **95**: 209–228.

Liang X, Lettenmaier DP, Wood EF, Burges SJ. 1994. A Simple hydrologically Based Model of Land Surface Water and Energy Fluxes for GSMs. *J. Geophys. Res.* **99**(D7): 14,415–14,428.

Liu J, Chen JM, Cihlar J, Park WM. 1997. A process-based boreal ecosystem productivity simulator using remote sensing inputs. *Remote Sensing of Environment* **62**: 158–175.

Manzoni S, Porporato A. 2007. Theoretical analysis of nonlinearities and feedbacks in soil carbon and nitrogen cycles. *Soil Biology & Biochemistry* **39**: 1542–1556.

McDonnell JJ, Sivapalan M, Vaché K, Dunn S, Grant G, Haggerty R, Hinz C, Hooper R, Kirchner J, Roderick ML, Selker J, Weiler M. 2007. Moving beyond heterogeneity and process complexity: a new vision for watershed hydrology. *Water Resources Research* **43**: W07301, DOI: 10.1029/2006 WR005467.

McEachern P, Prepas EE, Chanasyk DS. 2006. Landscape control of water chemistry in northern boreal streams of Alberta. *Journal of Hydrology* **323**: 303–324.

Mihailovic DT, Pielke RA, Rajkovic B, Lee TJ, Jeftic M. 1993. A resistance representation of schemes for evaporation from bare and partly plant-covered surfaces for use in atmospheric models. *Journal of Applied Meteorology* **32**: 1038–1054.

Montgomery D, Peck EA, Vining GG. 2001. *Introduction to Linear Regression Analysis*. Wiley: New York.

Morales P, Sykes MT, Prentice IC, Smith P, Smith B, Bugmann H, Zierl B, Friedlingstein P, Viovy N, Sabate S, Sanchez A, Pla E, Gracia CA, Sitch S, Arneth A, Ogee J. 2005. Comparing and evaluating process-based ecosystem model predictions of carbon and water fluxes in major European forest biomes. *Global Change Biology* **11**: 2211–2233.

Polcher J. 1995. Sensitivity of tropical convection to land surface processes. *Journal of Atmospheric Sciences* **52**(17): 3143–3161.

Porporato A, D'odorico P, Laio F, Rodriguez-Iturbe I. 2003. Hydrologic controls on soil carbon and nitrogen cycles. I. Modeling scheme. *Advances in Water Resources* **26**: 45–58.

Potter C, Klooster S, De Carvalho CR, Genovese VB, Torregrosa A, Dungan J, Bobo M, Coughlan J. 2001. Modeling seasonal and interannual variability in ecosystem carbon cycling for the Brazilian Amazon region. *Journal of Geophysical Research-Atmospheres* **106**: 10423–10446.

Renzetti AVE, Taylor, CH, Buttle JH. 1992. Subsurface flow in a shallow soil Canadian shield watershed. *Nordic Hydrology* **23**(4): 209–226.

Rodriguez-Iturbe I. 2000. Ecohydrology: a hydrologic perspective of climate-soil-vegetation dynamics. *Water Resources Research* **36**: 3–9.

Rodriguez-Iturbe I, D'Odorico P, Laio F, Ridolfi L, Tamea S. 2007. Challenges in humid land ecohydrology: interactions of water table and unsaturated zone with climate, soil, and vegetation. *Water Resources Research* **43**: W09301, DOI: 10.1029/2007WR006073.

Running SW. 1994. Testing Forest-Bgc ecosystem process simulations across a climatic gradient in Oregon. *Ecological Applications* **4**: 238–247.

Schulze ED, Kelliher FM, Korner C, Lloyd J, Leuning R. 1994. Relationships Among maximum stomatal conductance, ecosystem surface conductance, carbon assimilation rate, and plant nitrogen nutrition—a global ecology scaling exercise. *Annual Review of Ecology and Systematics* **25**: 629–660.

Shao Y, Henderson-Sellers A. 1996. Modeling soil moisture: a project for intercomparison of land surface parameterization schemes phase 2(b). *Journal of Geophysical Research* **101**: 7227–7250.

Shinozaki K, Yoda K, Hozumi K, Kira T. 1964. A quantitative analysis of plant form. Pipe model theory. I. Basic Analysis. *Japanese Journal of Ecology* **14**: 97–105.

Sitch S, Brovkin V, von Bloh W, van Vuuren D, Eickhout B, Ganopolski A. 2005. Impacts of future land cover changes on atmospheric CO_2 and climate. *Global Biogeochem. Cycles* **19**: GB2013, DOI:10.1029/2004GB002311.

Sonnentag O, Chen JM, Roulet NT, Ju W, Govind A. 2008. Spatially explicit simulation of peatland hydrology and carbon dioxide exchange: Influence of mesoscale topography. *J. Geophys. Res.* **113**: G02005, DOI:10.1029/2007JG000605.

Tague C, Band L. 2004. RHESSys: Regional Hydro-ecologic simulation system: An object-oriented approach to spatially distributed modeling of carbon, water and nutrient cycling. *Earth Interactions* **8**: 19, 1–42.

Thompson MV, Randerson JT, Malmstrom CM, Field CB. 1996. Change in net primary production and heterotrophic respiration: how much is necessary to sustain the terrestrial carbon sink? *Global Biogeochemical Cycles* **10**: 711–726.

Turner DP, Ritts WD, Styles JM, Yang Z, Cohen WB, Law BE, Thornton PE. 2006. A diagnostic carbon flux model to monitor the effects of disturbance and interannual variation in climate on regional NEP. *Tellus Series B-Chemical and Physical Meteorology* **58**: 476–490.

Vazquez RF, Feyen J. 2007. Assessment of the effects of DEM gridding on the predictions of basin runoff using MIKE SHE and a modelling resolution of 600 m. *Journal of Hydrology* **334**: 73–87.

Weiler M, McDonnell JJ. 2004. Virtual experiments: a new approach for improving process conceptualization in hill-slope hydrology. *Journal of Hydrology* **285**: 3–18, DOI: 10.1016/S0022-1694(03)00271-3.

Weiler M, McDonnell JJ, Tromp van Meerveld I, Uchida T. 2005. Subsurface Stormflow Runoff Generation Processes. In: *Encyclopedia of Hydrological Sciences*. M. G. Anderson, Editor. Wiley: Pp. 1719–1732.

Weiler M, McDonnell JJ. 2007. Conceptualizing lateral preferential flow and flow networks and simulating the effects on gauged and ungauged hillslopes. *Water Resources Research* **43**: W03403, DOI: 10.1029/2006 WR004867.

Wigmosta MS, Vail LW, Lettenmaier DP. 1994. A distributed hydrology-vegetation model for complex terrain. *Water Resources Research* **30**: 1665–1679.

Williams TG, Flanagan LB. 1998. Measuring and Modelling Environmental Influences on Photosynthetic Gas Exchange in Sphagnum and Pleurozium. *Plant Cell and Environment* **21**: 555–564.

Zgallai H, Steppe K, Lemeur R. 2006. Effects of severe water stress on partitioning of C-14-assimilates in tomato plants. *Journal of Applied Botany and Food Quality-Angewandte Botanik* **80**: 88–92.

Zimov SA, Schuur EAG, Chapin FS. 2006. Permafrost and the global carbon budget *Science* **312**: 1612–1613.